





Mixed anion control of negative thermal expansion in a niobium oxyfluoride†

 Eliza K. Dempsey ^{ab} and James Cumby ^{*ab}

 Cite this: *Chem. Commun.*, 2024, 60, 2548

 Received 15th December 2023,
 Accepted 1st February 2024

DOI: 10.1039/d3cc06129a

rsc.li/chemcomm

A significant change in thermal expansion with anion composition has been identified in the niobium oxyfluoride, $\text{NbO}_{2-x}\text{F}_{1+x}$ from $0 < x < 0.6$. Fluorine doping leads to a transition from positive thermal expansion to unusual zero and negative thermal expansion caused by transverse anionic vibrations. This work has consequences for the development of advanced technological materials with tuneable low thermal expansion and is the first example of the use of multiple anions to control thermal expansion.

Thermal expansion is often one of the most important engineering properties when considering materials for technological applications. In multi-component devices, such as a fuel cell which must undergo significant temperature changes, a mismatch in coefficient of thermal expansion (CTE) between materials can cause serious issues.^{1–3} In fields such as telescope optics, a component may be required to retain a precise shape over changes in temperature.^{4,5} Even the CTE of human teeth is considered when designing long lasting dental filling materials.^{6,7} These are just a few examples but there are many others where minimising or tuning CTE can significantly improve performance. A small minority of materials exhibit zero or negative thermal expansion (NTE), where the structure contracts on heating, however the number of available NTE materials is significantly limited and we have no robust method for designing new NTE materials.^{8,9}

NTE can originate due electronic or magnetic transitions, but the temperature range of NTE in these materials is limited.^{10,11} However, NTE over a broader temperature range is most commonly caused by transverse vibrations in flexible open framework structures.¹² The simplest example of structural NTE is in the cubic ReO_3 -type structure consisting of

corner-sharing octahedra (Fig. 1(A)). NTE can be theorised to arise in this structure due to tilting modes of the rigid octahedra according to the rigid unit mode (RUM) model.¹³ As the amplitude of the RUM vibration increases with temperature, the average cell volume decreases, resulting in NTE, as illustrated in Fig. 1(B).

Since the discovery of large NTE in ScF_3 in 2010,¹⁴ fluorides have become a rapidly growing area for discovery of new NTE materials.¹² Aside from ScF_3 , this has largely focused on double ReO_3 -type structures, such as CaZrF_6 , where the cations adopt a 3D “checkerboard” arrangement.^{15–17} Not all ReO_3 -type structures, however, exhibit NTE. In contrast to ScF_3 , ReO_3 only shows NTE over a limited temperature range.^{18,19} This has been attributed to reduced flexibility of oxide linkages compared to the highly flexible fluoride linkages in ScF_3 .^{20,21} The true NTE mechanism in these structures is likely to be more complex than a simple RUM model, with some evidence for non-rigid transverse phonons as the origin of NTE in ScF_3 .^{22,23}

Despite the growing number of oxide and fluoride based NTE materials,¹² little attention has so far been paid to mixed-anion oxyfluorides. ReO_3 -type NbO_2F and TaO_2F only exhibit positive and zero thermal expansion respectively despite their cubic structure.^{24,25} However, due to the variable oxidation state of niobium, the oxygen–fluorine ratio of NbO_2F can be modified to form the $\text{NbO}_{2-x}\text{F}_{1+x}$ solid solution whilst retaining the cubic structure.²⁶ This provides an excellent system for the



Fig. 1 (A) The cubic ReO_3 -type structure of NbO_2F in the $Pm\bar{3}m$ space group. (B) An illustration of the rigid unit mode mechanism of negative thermal expansion in the cubic ReO_3 -type structure.

^a School of Chemistry, University of Edinburgh, David Brewster Road, Edinburgh, EH9 3FJ, UK. E-mail: james.cumby@ed.ac.uk

^b Centre for Science at Extreme Conditions (CSEC), University of Edinburgh, Peter Guthrie Tait Road, Edinburgh EH9 3FD, UK

† Electronic supplementary information (ESI) available. See DOI: <https://doi.org/10.1039/d3cc06129a>



effects of mixed anions to be explored. Previously we have found a significant composition dependence of electronic and magnetic properties, driven by the substitution of Nb(v) for Nb(IV).²⁷

Through variable temperature X-ray powder diffraction, we have identified a significant change in the CTE of $\text{NbO}_{2-x}\text{F}_{1+x}$ when the fluorine content is increased, changing from positive to zero to negative thermal expansion. This presents a new pathway for precise tuning of thermal expansion through anionic composition and is, to our knowledge, the first example of an oxyfluoride NTE material.

$\text{NbO}_{2-x}\text{F}_{1+x}$ samples from $x = 0$ to $x = 0.6$ (*vide infra*) were synthesised by a high temperature solid state synthesis, full details of which are given in ESI.† Higher fluorine content compositions were achieved using polytetrafluoroethylene (PTFE) as a fluorine source. The use of PTFE provides a safer and cheaper alternative to fluoride synthesis than metal fluorides or hydrofluoric acid. The cubic ReO_3 -type structure and purity of our final products were confirmed from X-ray powder diffraction (ESI†). To characterise the thermal expansion properties of $\text{NbO}_{2-x}\text{F}_{1+x}$ X-ray powder diffraction data were collected at temperatures from 12–373 K. Low temperature data were collected in house with Cu- $\text{K}\alpha_1$ radiation whilst high temperature data were collected at the BM01 beamline of the European Synchrotron Radiation Facility (ESRF). The variation in unit cell volume was extracted from Rietveld refinements of the data using the GSAS-II software²⁸ and is shown in Fig. 2(A). Data for $\text{NbO}_{1.9}\text{F}_{1.1}$ between 200–250 K are unavailable due to sample misalignment during data collection. The mean and range of volumetric CTE for each composition is shown in Fig. 2(B).

The thermal expansion behaviour of NbO_2F is positive but shows an atypical levelling out at high temperature as previously reported.²⁴ This positive thermal expansion, when compared to reported zero thermal expansion in isostructural TaO_2F , was attributed to displacement of the central Nb ion.²⁵ In the case of $\text{NbO}_{1.9}\text{F}_{1.1}$, however, we observe near perfect zero thermal expansion from 12 to 310 K with a mean CTE of 0.4 ppm K^{-1} (ESI†). This presents a significant difference from NbO_2F despite only a subtle change to the overall chemical composition. We therefore believe this effect is structural rather than purely chemical in origin, with possible influence

from local structure or anion ordering due to the fluorine doping. The fact the thermal expansion shows no change over a broad temperature range indicates perfectly balanced positive and negative thermal expansion effects. Above 310 K, there is a clear switch to dominant positive thermal expansion.

Further fluoride doping, to form $\text{NbO}_{1.7}\text{F}_{1.3}$ and $\text{NbO}_{1.4}\text{F}_{1.6}$, leads to negative thermal expansion over the full measured temperature range (12 to 373 K). The NTE shows a clear correlation to fluoride doping (Fig. 2(B)) with mean volumetric CTEs of -3 and -5 ppm K^{-1} respectively. This is consistent with the larger flexibility of fluoride linkages in these structures compared to oxides. The increasing fluoride content softens the transverse anionic vibrations, allowing them to contribute to NTE without the overall cubic structure collapsing to a rhombohedral phase. This is similar to the mechanism of NTE observed in ScF_3 .

Refinement of the atomic displacement parameters for NbO_2F with temperature (Fig. 3(A)) gives similar results to those reported for TaO_2F .²⁵ As expected, the isotropic niobium displacement has a significant non-zero component independent of temperature, likely caused by local static displacements away from fluoride and towards oxide anions. The anion displacement, however, is strongly anisotropic and dominated by transverse displacement perpendicular to the Nb-(O/F)-Nb bond. This transverse anion displacement also shows a strong thermal dependence, increasing with temperature. The thermal dependence of this transverse displacement can be quantified from the gradient of a linear fit ($dU_{\text{transverse}}/dT$). By comparing these gradients for different $\text{NbO}_{2-x}\text{F}_{1+x}$ compositions (Fig. 3(B)) there is a clear correlation with a strong thermal dependence producing a more negative CTE. The strongly ionic nature of the fluoride bonding compared to more covalent oxide linkages increases the transverse flexibility of the anionic linkage, resulting in NTE. We have also extracted equivalent linear fit gradients from published ReO_3 -type and double ReO_3 -type displacement parameters. A comparison of our displacement gradients with these literature values show a similar correlation with CTE. We propose that this parameter is therefore a better measure of anion flexibility than the absolute transverse displacement parameter which may have both static



Fig. 2 (A) Relative variation in unit cell volume with temperature for $\text{NbO}_{2-x}\text{F}_{1+x}$ as determined from powder X-ray diffraction. (B) The range and mean values of volumetric coefficient of thermal expansion for each $\text{NbO}_{2-x}\text{F}_{1+x}$ composition.



Fig. 3 (A) Refined displacement parameters for NbO_2F . (B) The gradient of the transverse anion displacement parameter in ReO_3 -type structures showing its relationship with mean volumetric CTE.^{14,15,19,25,29–33} Linear fits were performed over the full temperature range of data available for which the structure remains cubic.



Table 1 Estimated composition of $\text{NbO}_{2-x}\text{F}_{1+x}$ samples as determined from the initial synthesis ratio, comparison of lattice parameters with literature values²⁶ and from magnetic susceptibility measurements

| Composition, x for $\text{NbO}_{2-x}\text{F}_{1+x}$ | | | |
|---|-----------------|---------------------------------|-------------------------|
| Sample ID | Synthesis ratio | Lattice parameter ²⁶ | Magnetic susceptibility |
| $x = 0.1$ | 0.19 | 0.04 | 0.07 |
| $x = 0.3$ | 0.31 | 0.37 | 0.24 |
| $x = 0.6$ | 0.63 | 0.43 | 0.57 |

and thermal contributions. This also supports the use of an anion-centred perspective to understand and control thermal expansion.

Determining the precise oxygen/fluorine composition in ceramic samples is a known challenge, therefore we have utilised a number of complementary approaches. Firstly, we have compared our refined lattice parameters with those reported by Brink *et al.* for $\text{NbO}_{2-x}\text{F}_{1+x}$ (ESI[†]).²⁶ Our results show slight deviation from our targeted compositions, likely due to the use of different synthesis procedures for high and low fluorine content samples which may lead to final compositions differing slightly from the idealised products. The corrected compositions, based on lattice parameters, are presented in Table 1. However these results may not be directly comparable due to the use of hydrofluoric acid in the Brink *et al.* synthesis which is known to lead to hydroxyl defects in the samples.²⁴ To support this analysis, we also performed magnetic susceptibility measurements with temperature (Fig. 4(A)). The high temperature, paramagnetic region is fitted to a Curie–Weiss model, $\chi_m = C/(T - \theta_w)$, in order to extract the paramagnetic moment (Fig. 4(B)). Therefore, the percentage of Nb^{4+} and composition of each sample could be determined. Full details of the analysis are provided in ESI.[†] The results of both these approaches, presented in Table 1, show reasonable agreement with each other and with the composition of starting products allowing us to estimate composition to within 0.1.

In summary, we have identified a novel approach to controlling thermal expansion through varying the oxygen to fluorine ratio. Only small changes in anion composition dramatically alter the CTE from positive to zero to negative with the effect persisting over a broad temperature range (12 to 373 K). To our knowledge, this is the first example of negative thermal expansion in an

oxyfluoride material with a notable negative CTE of -5 ppm K^{-1} in $\text{NbO}_{1.4}\text{F}_{1.6}$. This highlights the importance of often overlooked anionic contributions and the great potential of mixed anion materials which have already been highlighted for use in fields such as battery electrodes, photocatalysis and optics.^{34–39} We anticipate this work will lead to a new class of metal oxyfluorides with tuneable low thermal expansion in combination with functional optical, magnetic and electronic properties.

EKD and JC jointly conceptualized the study and devised the methodology. EKD led the investigation, developed visualizations and wrote the original draft. JC provided resources, supervision and edited the manuscript.

EKD wishes to thank the University of Edinburgh for funding. We would like to thank Dr Charlie McMonagle (ESRF) and Dr Rebecca Rae (CSEC) for assistance with data collection. For the purpose of open access, the author has applied a Creative Commons Attribution (CC BY) licence to any Author Accepted Manuscript version arising from this submission.

Conflicts of interest

There are no conflicts to declare.

Notes and references

- J. Kim and A. Manthiram, *Chem. Mater.*, 2010, **22**, 822–831.
- C. S. Montross, H. Yokokawa and M. Dokiya, *Br. Ceram. Trans.*, 2002, **101**, 85–93.
- Y. Zhang, B. Chen, D. Guan, M. Xu, R. Ran, M. Ni, W. Zhou, R. O'Hayre and Z. Shao, *Nature*, 2021, **591**, 246–251.
- T. Legero, T. Kessler and U. Sterr, *J. Opt. Soc. Am. B*, 2010, **27**, 914–919.
- C. Blaurock, M. McGinnis, K. Kim and G. E. Mosier, *Proc. SPIE*, 2005, **5867**, 58670V.
- M. B. Lopes, Z. Yan, S. Consani, A. Gonini Júnior, A. Aleixo and J. F. McCabe, *Braz. Dent. J.*, 2012, **23**, 03–07.
- H. Wolter, W. Storch and H. Ott, *MRS Online Proc. Libr.*, 1994, **346**, 143–149.
- C. Lind, *Materials*, 2012, **5**, 1125–1154.
- A. W. Sleight, *Curr. Opin. Solid State Mater. Sci.*, 1998, **3**, 128–131.
- E. Pachoud, J. Cumby, C. T. Lithgow and J. P. Attfield, *J. Am. Chem. Soc.*, 2018, **140**, 636–641.
- Y. Song, N. Shi, S. Deng, X. Xing and J. Chen, *Prog. Mater. Sci.*, 2021, **121**, 100835.
- N. Shi, Y. Song, X. Xing and J. Chen, *Coord. Chem. Rev.*, 2021, **449**, 214204.
- M. T. Dove, K. O. Trachenko, M. G. Tucker and D. A. Keen, *Rev. Mineral. Geochem.*, 2000, **39**, 1–33.
- B. K. Greve, K. L. Martin, P. L. Lee, P. J. Chupas, K. W. Chapman and A. P. Wilkinson, *J. Am. Chem. Soc.*, 2010, **132**, 15496–15498.
- J. C. Hancock, K. W. Chapman, G. J. Halder, C. R. Morelock, B. S. Kaplan, L. C. Gallington, A. Bongiorno, C. Han, S. Zhou and A. P. Wilkinson, *Chem. Mater.*, 2015, **27**, 3912–3918.
- B. R. Hester, J. C. Hancock, S. H. Lapidus and A. P. Wilkinson, *Chem. Mater.*, 2017, **29**, 823–831.
- L. Hu, J. Chen, J. Xu, N. Wang, F. Han, Y. Ren, Z. Pan, Y. Rong, R. Huang, J. Deng, L. Li and X. Xing, *J. Am. Chem. Soc.*, 2016, **138**, 14530–14533.
- T. Chatterji, T. C. Hansen, M. Brunelli and P. F. Henry, *Appl. Phys. Lett.*, 2009, **94**, 241902.
- T. Chatterji, P. F. Henry, R. Mittal and S. L. Chaplot, *Phys. Rev. B: Condens. Matter Mater. Phys.*, 2008, **78**, 134105.
- T. A. Bird, M. G. L. Wilkinson, D. A. Keen, R. I. Smith, N. C. Bristowe, M. T. Dove, A. E. Phillips and M. S. Senn, *Phys. Rev. B: Condens. Matter Mater. Phys.*, 2021, **104**, 214102.

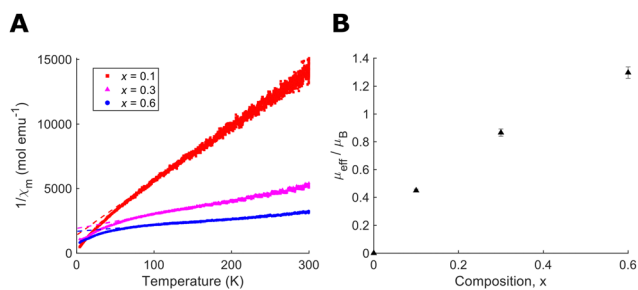


Fig. 4 (A) Inverse magnetic susceptibility against temperature for $\text{NbO}_{2-x}\text{F}_{1+x}$ including linear Curie–Weiss fits. Diamagnetic and ferromagnetic corrections have been applied. (B) Effective magnetic moments calculated from Curie–Weiss fitting.



- 21 T. A. Bird, J. Woodland-Scott, L. Hu, M. T. Wharmby, J. Chen, A. L. Goodwin and M. S. Senn, *Phys. Rev. B*, 2020, **101**, 064306.
- 22 L. Hu, J. Chen, A. Sanson, H. Wu, C. Guglieri Rodriguez, L. Olivi, Y. Ren, L. Fan, J. Deng and X. Xing, *J. Am. Chem. Soc.*, 2016, **138**, 8320–8323.
- 23 M. T. Dove, *Philos. Trans. R. Soc., A*, 2019, **377**, 20180222.
- 24 A. P. Wilkinson, R. E. Josefsberg, L. C. Gallington, C. R. Morelock and C. M. Monaco, *J. Solid State Chem.*, 2014, **213**, 38–42.
- 25 J. Z. Tao and A. W. Sleight, *J. Solid State Chem.*, 2003, **173**, 45–48.
- 26 F. J. Brink, L. Norén and R. L. Withers, *J. Solid State Chem.*, 2004, **177**, 2177–2182.
- 27 E. K. Dempsey and J. Cumby, *J. Mater. Chem. C*, 2023, **11**, 1791–1797.
- 28 B. H. Toby and R. B. Von Dreele, *J. Appl. Crystallogr.*, 2013, **46**, 544–549.
- 29 B. R. Hester and A. P. Wilkinson, *Inorg. Chem.*, 2018, **57**, 11275–11281.
- 30 L. Hu, J. Chen, L. Fan, Y. Ren, Y. Rong, Z. Pan, J. Deng, R. Yu and X. Xing, *J. Am. Chem. Soc.*, 2014, **136**, 13566–13569.
- 31 J. Xu, L. Hu, L. Wang, J. Deng, J. Chen and X. Xing, *Acta Phys. – Chim. Sin.*, 2018, **34**, 339.
- 32 C. R. Morelock, B. K. Greve, L. C. Gallington, K. W. Chapman and A. P. Wilkinson, *J. Appl. Phys.*, 2013, **114**, 213501.
- 33 B. K. Greve, PhD Thesis, Georgia Institute of Technology, 2012.
- 34 H. Kageyama, K. Hayashi, K. Maeda, J. P. Attfield, Z. Hiroi, J. M. Rondinelli and K. R. Poeppelmeier, *Nat. Commun.*, 2018, **9**, 772.
- 35 M. A. Lange, I. Khan, R. Dören, M. Ashraf, A. Qurashi, L. Prädél, M. Panthöfer, M. von der Au, A. Cossmer, J. Pfeifer, B. Meermann, M. Mondeshki, M. N. Tahir and W. Tremel, *Dalton Trans.*, 2021, **50**, 6528–6538.
- 36 M. A. Lange, I. Khan, P. Opitz, J. Hartmann, M. Ashraf, A. Qurashi, L. Prädél, M. Panthöfer, A. Cossmer, J. Pfeifer, F. Simon, M. von der Au, B. Meermann, M. Mondeshki, M. N. Tahir and W. Tremel, *Adv. Mater.*, 2021, **33**, 2007434.
- 37 H. Mizoguchi, M. Orita, M. Hirano, S. Fujitsu, T. Takeuchi and H. Hosono, *Appl. Phys. Lett.*, 2002, **80**, 4732–4734.
- 38 N. H. Bashian, M. B. Preefer, J. Milam-Guerrero, J. J. Zak, C. Sendi, S. A. Ahsan, R. C. Vincent, R. Haiges, K. A. See, R. Seshadri and B. C. Melot, *J. Mater. Chem. A*, 2020, **8**, 12623–12632.
- 39 L. Permér, *J. Solid State Chem.*, 1992, **97**, 105–114.

